NANO LETTERS

2007
Vol. 7, No. 12
3832−3839

Triplex Addressability as a Basis for Functional DNA Nanostructures

John Tumpane,[†] Ravindra Kumar,[‡] Erik P. Lundberg,[†] Peter Sandin,[†] Nittaya Gale,[‡] Iris S. Nandhakumar,[‡] Bo Albinsson,[†] Per Lincoln,[†] L. Marcus Wilhelmsson,[†] Tom Brown,[‡] and Bengt Nordén*,[†]

Department of Chemical and Biological Engineering/Physical Chemistry, Chalmers University of Technology, SE-41296 Gothenburg, Sweden, and School of Chemistry, University of Southampton, Highfield, Southampton SO17 1BJ, UK

Received October 1, 2007; Revised Manuscript Received October 22, 2007

ABSTRACT

Here, we present the formation of a fully addressable DNA nanostructure that shows the potential to be exploited as, for example, an information storage device based on pH-driven triplex strand formation or nanoscale circuits based on electron transfer. The nanostructure is composed of two adjacent hexagonal unit cells (analogous to naphthalene) in which each of the eleven edges has a unique double-stranded DNA sequence, constructed using novel three-way oligonucleotides. This allows each ten base-pair side, just 3.4 nm in length, to be assigned a specific address according to its sequence. Such constructs are therefore an ideal precursor to a nonrepetitive two-dimensional grid on which the "addresses" are located at a precise and known position. Triplex recognition of these addresses could function as a simple yet efficient means of information storage and retrieval. Future applications that may be envisaged include nanoscale circuits as well as subnanometer precision in nanoparticle templating. Characterization of these precursor nanostructures and their reversible targeting by triplex strand formation is shown here using gel electrophoresis, atomic force microscopy, and fluorescence resonance energy transfer (FRET) measurements. The durability of the system to repeated cycling of pH switching is also confirmed by the FRET studies.

Introduction. The technological age calls for ever more efficient and increasingly smaller structures on which applications can be based. This has meant that in recent years there is a marked shift from research in top-down approaches to bottom-up strategies within the field of nanotechnology with bottom-up being more genuinely "nanoscale". It is therefore imperative to find materials and substrates that are amenable to bottom-up nanoscale research. Self-assembly is the key element to this design whereby molecules come together in a deliberate, predesigned fashion to construct the specified nanostructure. DNA is an obvious candidate, efficiently used in nature for millions of years to encode information in an extremely densely packed fashion and with an unrivalled fidelity to design and assembly. The exploitation of nucleic acids as a nanomaterial is a rapidly expanding field, led by the pioneering work of the Seeman group.[1−3] DNA is favored due to the inherent encodability afforded by the four-base alphabet (A, G, C, T) and the fact that normal B-DNA duplexes are built up with a mere 3.4 Å between each base-pair, allowing subnanometer precision in functionalization provided one can manage to addressably and specifically target this at the single base level. Nanoconstruction using nucleic acids has not just been limited to planar arrays but has also ventured into three-dimensional structures,[4−6] DNA nanotubes,[7,8] and even the RNA world.[9] Stojanovic et al. have employed DNA as a basis for molecular logic gates and used them to perform what are relatively complex functions, proving the suitability of DNA as a computational alternative.[10] Recent advances have also seen the realization of smaller DNA nanostructures as a template for molecular lithography.[11,12]

Two-dimensional (2D) arrays or networks of DNA nanostructures are a potentially very exciting facet of nanotechnology because of their obvious compatibility with surface immobilization and ease of self-assembly. However, for their potential to be fully exploited and indeed their functionalization to be nonredundant, it must be necessary to build and tune them in a nonrepetitive manner.[13] A nonperiodic net infers that functionalities can be situated in specific (unambiguous) points and in a determined pattern, that is, so that a circuit or pathway with known directionality can be constructed across the array. This is imperative if one is to use such networks for, for example, energy transport or information storage and retention. It is therefore necessary to devise a way to self-assemble these kinds of networks in a facile, efficient, and predictable manner. The purpose of our current study is to design, characterize, and address a simple but nonrepetitive structure to demonstrate the potential

* Corresponding author. Email: norden@chalmers.se. Telephone: +46-(0)31-7723041. Fax: +46-(0)31-7723858.
[†] Chalmers University of Technology.
[‡] University of Southampton.

10.1021/nl072512i CCC: $37.00
Published on Web 11/06/2007

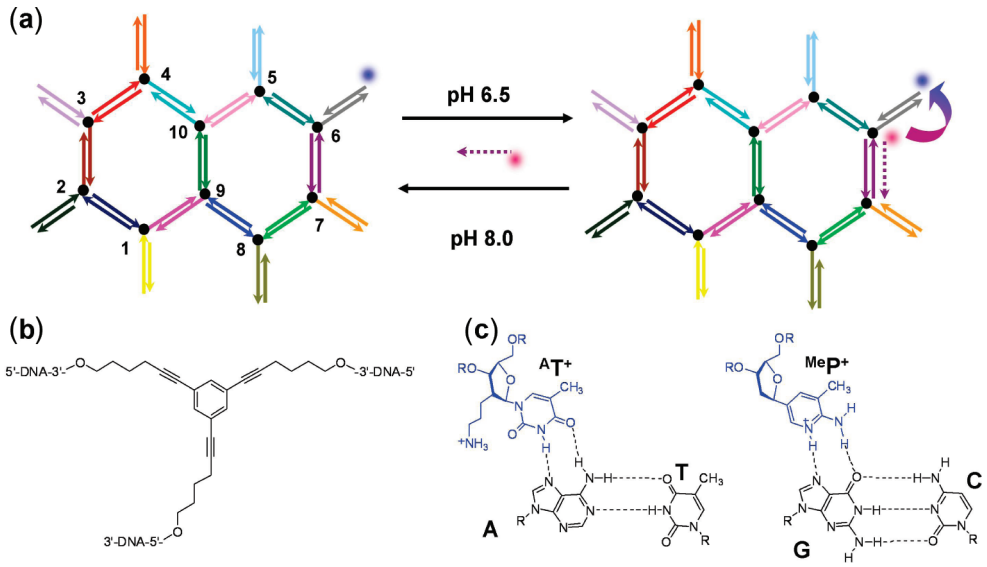

Figure 1. (a) Schematic graphic of the nanostructure, left. Each ten-mer side is composed of a unique sequence, orthogonal to all the other sequences, as indicated by the color-coding. The arrowheads indicate the 3′-terminus of each arm, and the three-way oligonucleotides are numbered at their nodal points depicted as black circles. The side-arms form double-strands (dsDNA) with normal ten-mer oligos that can be labeled with fluorophores, etc., but obviously more trigonal junctions can be used to build more extensive structures. The pH-dependent binding of the triplex strand is shown to the right with the TFO shown as a dashed purple line; this is labeled at the 5′-terminus with a Cy3 fluorophore (pink), and for the FRET studies the peripheral arm at node 6 is labeled with Cy5 (blue). (b) The 1,3,5-trihex-1-ynylbenzene based node. (c) ^{A}T·AT triplet (left) and ^{Me}P·GC triplet (right). The TFO bases are shown in blue and the duplex bases in black.

inherent in such arrays. To this end we propose a fused pseudo-bihexagonal structure; see Figure 1 , which is referred to as "naphthalene" and based on the previously reported "benzene",[14] (borrowing from the nomenclature first coined by von Kiedrowski[15]). The nanoconstruct is built from ten different three-way DNA nodes (branched oligonucleotides, Figure 1b), which provide rich information content. Each ten-mer side is unique and is in principle selectively addressable by triplex formation with the structure also bearing eight unique peripheral side-arms that can be used to extend the network in a nonrepetitive manner. Alternatively, these peripheral arms can themselves be addressed by duplex formation with labeled complementary oligonucleotides.

As one way of addressing our proposed nanostructures at specific loci, we have chosen to employ triplex recognition to deliver one of the functionalities to the system. Triplex strand addressability is an interesting concept for several reasons. First, it is an elegant and simple way to specifically target a defined sequence, and second it is easily controlled by a change in pH of the system with the triplex being most stable at low pH. This means that one has a system that can be steered by temperature, pH, ionic strength, and even photophysically by the use of fluorophores. The triplex-forming oligonucleotide (TFO) can itself be labeled with a variety of molecules (fluorophores, electron-transfer moieties, etc.), so this simple strategy can form the basis of many applications while maintaining the simplicity and fidelity of the system. The triplex approach to DNA sequence recognition has been studied for many years, and it is well established that a suitable third strand of DNA is known to be able to bind to a Watson−Crick base-paired duplex via Hoogsteen base-paring in the major groove. A sequence-specific interaction has recently been developed to provide recognition of all four Watson−Crick base pairs, allowing any sequence of double-stranded DNA to be addressed, and is therefore ideal for the current purpose. Very stable triplexes can be formed between a pyrimidine-rich TFO and a DNA duplex with one polypurine strand and one polypyrimidine strand although this is not a prerequisite when using full-recognition TFOs.[16] The TFO is oriented parallel to the purine strand of the duplex to which it binds via Hoogsteen bonding. Triplex binding is greatly enhanced if the TFO contains units that are easily protonated at an acidic pH with the positive charge reducing the destabilizing repulsion between the phosphate backbones of the three component strands. In this work we use ^{A}T (2′-aminoethoxythymidine) to recognize AT base pairs[17] and ^{Me}P (3-methyl-2-aminopyridine) to recognize GC[18,19] (Figure 1c). The triplex-binding properties of strands containing these modifications have been well characterized.[20] Because of the reliance on protonation, binding of such TFOs is stabilized at low pH and reversed by increasing the pH. ^{A}T promotes triplex stability by protonation of the 2′-amino group attached to the sugar, which forms a stable interaction with the anionic phosphodiester groups of the duplex.[21] At high pH, the amine is deprotonated, and this enhances the effectiveness of the triplex pH switch. ^{Me}P forms two hydrogen bonds with the guanine base of a GC base pair, and one of these (N1H of protonated ^{Me}P^{+} to N7 of guanine, Figure 1c) is lost at high pH and the triplex becomes unstable. The pK_a of N1 of ^{Me}P is 6.1, so the contribution of ^{Me}P to the pH switch is most effective just above pH 6. Because of the above factors, triplex binding is very sensitive to small changes in pH that can bring about site-specific labeling or dissociation of suitably designed DNA nanostructures.

Triplex-binding strategies have been used before as a means of labeling nanonetworks[22] with, for example, gold nanoparticles,[23] but this is the first time that triplex recognition has been used to label and functionalize nanostructures with such a level of addressability and spatial precision. This strategy is a simple model of a write−read−erase function of an information-rich DNA nanostructure driven by changes in pH.

Our previous work demonstrates the principle of addressability by the selective labeling of a single nanostructure by fluorophores.[14] Here, we further explore this concept by constructing the first in a new generation of extended, information-rich nonrepetitive nanostructures. This nanostructure now contains two nonidentical pseudo-hexagonal unit cells where each edge is unique. Thus, while geometrically identical and symmetrical, the subunits of the nanoconstruct are individually distinct and addressable at each specific point.

Method. *DNA Sequence Design.* Each 10-mer sequence was designed to be sequence orthogonal to all others with the requirements that no more than four consecutive bases of any sequence are complementary to any part of any other sequence. Where possible, the number of GC base pairs was increased to ensure high-melting temperatures. The sequences were assigned to each node with the criterion that there be little possibility for hairpin structures between arms on the same node where directionality and close proximity might favor the formation of such structures. One 10-mer sequence was designed to be a polypurine, and its complementary sequence a polypyrimidine to be suitable for triplex targeting.

Synthesis of Oligonucleotides. The detailed synthesis of the trigonal oligonucleotides has been described previously (Supporting Information in reference 14). Briefly, synthesis of the trigonal oligonucleotide constructs (Figure 1b) was carried out by standard solid-phase methods on an ABI-394 automated synthesizer. The first arm was assembled, and then the nodal 1,3,5-tri(hex-1-ynyl)benzene phosphoramidite monomer was incorporated. Standard synthesis was continued from this point to grow the second arm, which was capped at its 5′-end to prevent further extension. The levulinoyl protecting group on the remaining unextended side arm of the node was then removed by treatment of the DNA synthesis column with hydrazine in pyridine/acetic acid, and the third arm was assembled by automated synthesis. The fully formed branched oligomer was then cleaved from the column and deprotected by heating in concentrated aqueous ammonia at 55 °C for 5 h. All oligonucleotides were purified by reversed-phase high-performance liquid chromatography. Branched oligonucleotides assembled in this way have two of the arms attached to the nodal derivative at their 3′ termini and the third at the 5′ terminus. Other strand orientations are possible if one or more of the arms is synthesized in the opposite direction using reverse amidites (Link Technologies Ltd, Glasgow, UK). Standard 10-mer sequences, complementary to the exterior arms of the structures were also synthesized as normal oligonucleotides and/or as a 5′-Cy3 or Cy5-labeled oligonucleotides by the standard automated solid-phase phosphoramidite method. Synthesis of TFOs has been described previously.[20,24] The following TFO sequence was chosen: 5′-Cy3- $^{A}T^{Me}P^{A}T^{A}T^{Me}P^{A}T^{A}T^{Me}P^{A}T^{Me}P$-3′-propanol where ^{Me}P is 3-methyl-2aminopyridine-2′-deoxyribonucleoside[19] and ^{A}T is 2′-aminoethoxythymidine.[17] This parallel TFO was designed to target the purine strand 5′-AGAAGAAGAG-3′ of the duplex on side 6-7 of the naphthalene construct (Figure 1a) at low pH by formation of $^{A}T^{+}$·AT and $^{Me}P^{+}$·GC triplets (Figure 1c).

Nanoconstruct Preparation. All oligonucleotides were prepared as 2 μM solutions in phosphate buffer (200 mM Na^{+}, pH 7.5) using their A_{260} values except for the Cy3 labeled strands where their A_{552} values were used instead. The pseudo-hexagonal nanostructures were then prepared by mixing equal volumes of each component oligonucleotide, heating to 80 °C, and allowing to cool to room temperature overnight. Final concentration was approximately 100 nM [naphthalene-construct]. This is a simple and efficient means of self-assembly and has previously given extremely high yields.[14] The triplex-addressed structures were assembled in the same way but using a phosphate/citrate buffer at pH 6.3 (200 mM Na^{+}) and 1.25 equiv. of the triplex-forming strand and a total construct concentration of 50 nM.

Gel Electrophoresis. To confirm the formation of the nanoconstructs, they were subjected to submerged gel electrophoresis using 4.5% MetaPhor agarose at 4 °C for 3−4 h at a field strength of 4.3 V cm^{-1} in the same phosphate or phosphate/citrate buffers, respectively. Imaging was carried out on a FluorImager 595 (Molecular Dynamics) via detection of the emission from the Cy3 labels (λ_{ex} = 514 nm, 570 ± 15 nm band-pass filter). Emission from Cy5 was imaged on a Storm scanner (Molecular Dynamics) with red fluorescence detection (λ_{ex} = 635 nm). The gels for the triplex-targeting experiments were cast as 4.5% MetaPhor in the pH 7.5 buffer and then steeped overnight in the pH 6.3 buffer before being subjected to electrophoresis in this lower pH buffer for 3 h. This was to ensure comparability and consistency with respect to pore size. After initial scanning, this gel was then reimmersed in the pH 7.5 phosphate buffer to destabilize the triplex strand but not the nanostructures themselves and subjected to electrophoresis for a further 2 h. Fluorescence intensities over the band volumes were estimated using the ImageQuant software (Molecular Dynamics) and subtracting the gel's natural background.

Fluorescence Resonance Energy Transfer. Fluorescence spectra were recorded on a Spex Fluorolog 3 spectrofluorimeter (JY Horiba) at 7 °C. Cy3 was excited at 510 nm and the direct excitation spectra of Cy5 (see Supporting Information) at 610 nm. The naphthalene construct bearing the Cy3-labeled TFO on side 6-7 (Figures 1 and 3) and the Cy5-labeled 10-mer on peripheral arm 6 is referred to as **T6**. The sample **T6**, which is the same as in the electrophoresis measurements (Figure 3), was taken, and the pH then switched between 6 and 8 by addition of either a 5 M NaOH or 5 M HCl solution (1 μL aliquots to an initial volume of 60 μL). Initial concentration was approximately 50 nM [naphthalene-construct]. This switching was cycled

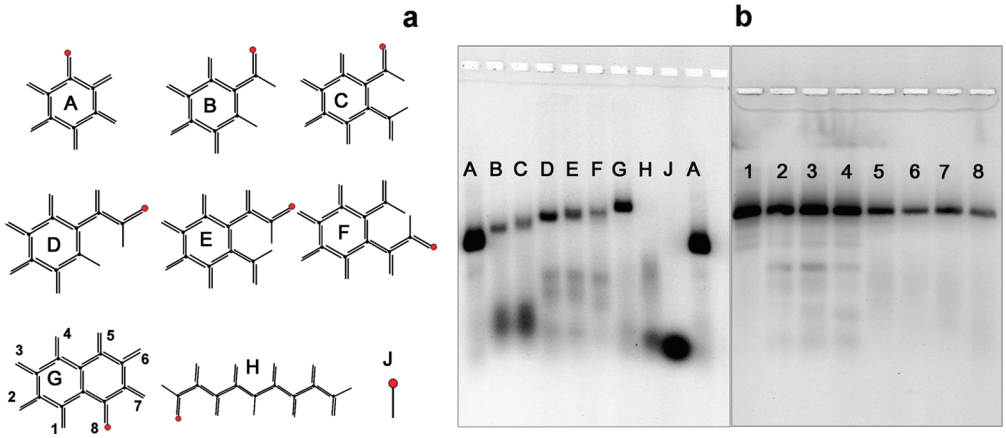

Figure 2. (a) The stepwise construction of a double-pseudo-hexagon. Structures **A**−**J** are indicated in the schematic on the left. Gel electrophoresis was performed in 4.5% MetaPhor agarose in a phosphate buffer (pH 7.5, 200 mM Na^+). The red dots indicate the position of the Cy3 fluorophore label, which was used for imaging. (b) Duplex addressability of the naphthalene construct. Each lane shows the same construct, **G**, labeled with Cy3 but with this fluorophore sited at a different sidearm in each case, as indicated by the numbers in the schematic, **G**.

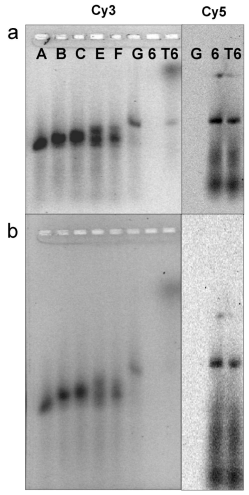

Figure 3. Gel electrophoresis shows the selective binding of a TFO at pH 6.3. Lanes **A**−**G** correspond to the same structures as in Figure 2. (a) After electrophoresis at pH 6.5 for 3 h. The same gel is imaged for Cy3, shown left and for Cy5, shown right. Construct **G** (labeled with Cy3 only at arm **1)**, **6** (labeled at arm 6 by Cy5), and **T6** (same as **6** but with the Cy3 labeled TFO) all correspond to the naphthalene construct. Lane **T6** shows that the naphthalene containing band has fluorescence from both Cy3 and Cy5 and therefore the TFO must be bound to the correct structure. Excess TFO appears as the diffuse, slow-migrating band of lane **T6** in the Cy3 scans. (b) After reimmersion in pH 7.5 buffer and 2 subsequent hours of electrophoresis. The naphthalene band in lane **T6** now only shows fluorescence from Cy5 indicating that the TFO has been detached, and the unbound TFO appears streaked in the Cy3 image after detachment.

3 times with approximate half hour intervals between switching steps.

Results. The gel electrophoresis results in Figure 2a show the stepwise construction of the naphthalene nanostructure. Starting from the left, the lanes contain the original pseudo-hexagonal structure (**A**),[14] and then a subsequent three-way oligonucleotide is added progressively in each lane (**B**−**F**) until the naphthalene structure (**G**) is completed. As more trigonal nodes are added, the mobility in the gel decreases, and we see clear separation between all these bands despite only minor changes in geometry and increasing charge. One can clearly see the formation of structures composed of six (benzene, nodes **1**−**4**, **9**, **10**, numbering as in Figure 1), seven (nodes **1**−**5**, **9**, **10**), eight, nine and ten nodes (naphthalene, nodes **1**−**10**) in the bands of the gel. This confirms that it is possible to build on from the initial structure and that all nodes are contained within the same structure. The question might remain as to if the new naphthalene structure is really composed of two ring-closed pseudo-hexagons or if only one of them is closed. Looking at lanes **E** and **F** in the gel, we see that even building on from the original construct in either the clockwise or counter-clockwise direction to form a nine-node structure yields the same result that is different from those containing only eight of the nodes (**C** and **D**). Therefore nodes **5** and **8** must be entirely double-stranded and connected to nodes **6** and **7** leaving the middle sequence connecting nodes **6** and **7** (purple in Figure 1a) as the only possible link in the chain that may not be double-stranded. Now, it is reasonable to assume that this is also double-stranded because the mobility in the gel is significantly different to the other structures and there is only one band present, which excludes an equilibrium of open and closed structures, but conveniently this is also the proposed target site of the triplex-strand, consisting of one all-purine and one all-pyrimidine strand. Superficial inspection of these sequences might indicate that it is less stable due to lower GC content so it is important to confirm that the triplex strand can bind in order to know that all sides really are double-stranded and that the proposed structure is the correct one (see below).

The second gel, Figure 2b, shows the same naphthalene structure, **G**, in all lanes but where each lane contains the construct labeled at a different position with a Cy3 fluorophore. This gel therefore shows the selective labeling of eight specific addresses (duplex addressability) on the construct. All constructs are labeled at the 5′-terminus of the 10-mer sequence with Cy3. It is clearly seen that the same construct is formed in each case, corresponding to a characteristic band

in the lanes and that the yield is relatively high in all cases. It is interesting to note the slight difference in intensity between the first set of labels (**1**−**4**) where the 5′ labeling places the fluorophore near the tri-hex-1-ynyl-benzene nodal point and the second set (**5**−**8**) where the directionality of the oligonucleotide arms has been reversed and the 5′ Cy3 label now sits on the exterior at the terminus of each arm (indicated by the arrowheads in **Figure 1b**). This may be due to a change in fluorescence quantum yield depending on the environment of the fluorophore, which obviously is quite different in these two situations.

The result of the electrophoresis experiment to explore triplex addressability can be seen in Figure 3a where a similar pattern is obtained for all constructs (**A**−**E**, **G**) as in Figure 2a. The triplex strand, TFO, labeled with Cy3 migrates with the naphthalene construct, **6**, which is only labeled by Cy5, when combined in lane **T6** which shows a band with equal mobility to that known to be the naphthalene structure, **G**, indicating that they must definitely form part of the same structure and that the targeting strand has bound. Emission from Cy5 is also seen from the same band in lane **T6** thus confirming that it is one single band corresponding to one single structure and that this structure is the naphthalene construct. This is indeed proof that the triplex binds to the constructs as desired and that all sides of the "naphthalene" construct are actually closed. The intensity over the volume of this band in **T6** is approximately 20% of that in lane **G**, indicating a high yield of triplex formation even though only a slight excess of TFO was used and that fluorescence intensity in the band is greatly reduced because of the occurrence of FRET. It is interesting to note that in this case the very short triplex-binding strand migrates much slower than the appreciably larger nanostructures with many more base-pairs and that there is no overlap between the TFO band and the naphthalene-bound TFO band in **T6**. This is because the protonation of the bases greatly reduces the overall charge of the triplex single-strand, and it therefore has a greatly retarded mobility in the gel. When reimmersed in a pH 7.5 buffer and subjected to further electrophoresis, it can be seen that after 2 h the Cy3 band in lane **T6**, which appears faint and streaked behind the construct band, no longer has the same mobility as the naphthalene construct, **6**, nor as the Cy5 band because the triplex formation is hindered at this more basic pH and the triplex addressability has been deliberately removed. Running the same gel entirely at pH 7.5 proves that the triplex-strand does not bind at higher pH since we see the presence of a band in the gel corresponding to the individual triplex-forming strand and no construct-bound TFO band (data not shown).

Association and dissociation of the triplex-forming strand to its target address on the naphthalene construct was also monitored in solution by fluorescence resonance energy transfer measurements. The comparison of the energy transfer at low pH (triplex formed) and high pH (triplex-forming strand dissociates from naphthalene) is shown in terms of acceptor fluorescence intensity in Figure 4. The spectra show the acceptor (Cy5) emission upon direct excitation of the donor (Cy3) in sample **T6**. These spectra are obtained by

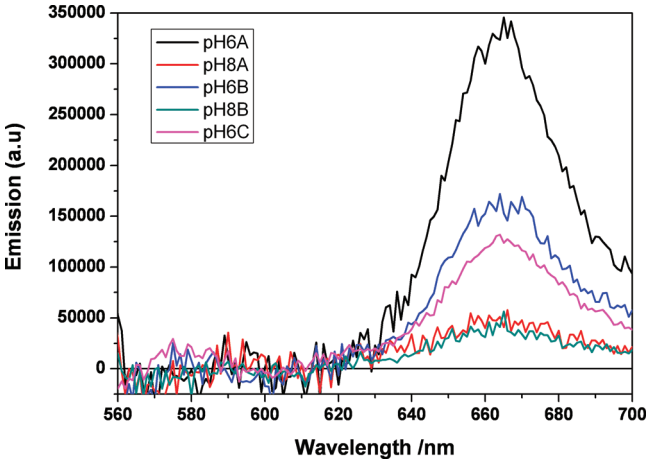

Figure 4. Recovered acceptor (Cy5) emission spectra (see text and Supporting Information for details about the recovery) for sample **T6** as in Figure 3. The initial fluorescence intensity is given as pH6A (black line) and subsequent pH switching to pH 8 (red line), switching back to pH 6 (blue line) and an additional cycle of the system to pH 8 (green line) and back to pH 6 (pink line). There is a clear on/off effect of pH switching on FRET despite some loss in total intensity due to loss of material.

first fitting a standard, measured, Cy3 emission spectrum to a part of the measured emission spectrum where only Cy3 emission is present, which in our case is between 560 and 610 nm, and then numerically subtracting it (see Supporting Information for details). This leaves only the Cy5 emission resulting from FRET and a minute effect of direct excitation of Cy5 at this excitation wavelength, 510 nm. The contribution of the latter is of very small amplitude (see green and red lines in Figure 4). The construct used corresponds to the band in lane **T6**, Figure 3a, where the TFO is Cy3 labeled and naphthalene is Cy5 labeled at position **6** as indicated in the graphic in Figure 1. Cy3 and Cy5 were chosen as they are known to be relatively pH insensitive in the pH range 3−10, and control experiments on the TFO strand confirmed that in the pH range 6−8 there is no visible effect on its fluorescence intensity.

In Figure 4, the black line, pH6A, clearly shows energy transfer between Cy3 and Cy5 at pH 6 where the triplex-targeting strand is bound to the naphthalene construct, positioning the FRET chromophores in close proximity to one another. FRET can only take place when the TFO is bound to the naphthalene structure in which Cy3 and Cy5 are positioned close enough for energy transfer to occur. Changing the pH to 8 (red line) causes a significant decrease in the acceptor intensity; in fact, the intensity is similar to what is expected to arise from direct excitation of Cy5. There is no doubt that the energy transfer is absent at this pH, proving that the TFO does not bind to the nanostructure. When reversing the pH to 6 again (blue line), the FRET signal returns indicating that the TFO again binds to the naphthalene structure. The obvious loss of intensity when comparing pH6A and pH6B is also seen in the spectra obtained when exciting Cy5 directly at 610 nm (where Cy3 does not absorb, see Supporting Information). This indicates a loss of DNA material in the pH cycling. We will return to this in the discussion. Nevertheless, the data show a

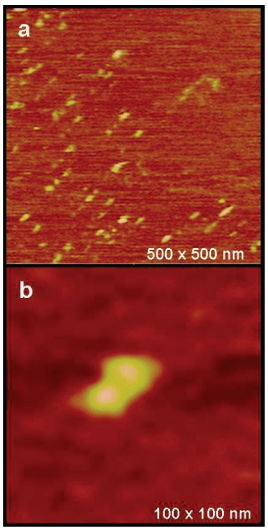

Figure 5. AFM images show the topography of these nanostructures in a buffer solution on mica. In the enlarged area, naphthalene construct (**G**) appears as an oblong structure (like a filled-in figure of eight) approximately 10 × 20 nm.

significant on/off change in FRET when switching between pH 6 and 8 demonstrating successful binding and unbinding of the TFO to the nanostructure. The cycle is repeated one more time (pH6B to pH8B and back to pH6C), and once again the FRET signal disappears at pH 8 and reappears at pH 6 as the TFO dissociates and associates to the nanostructure. The data in the graph show that the system can be switched three times between the off and on FRET states although preliminary results suggest that these cycles can be repeated an even greater number of times.

The rough topology of the nanostructure, **G**, is revealed by the AFM images in Figure 5b where they appear as a sort of filled-in figure-of-eight shape. The dimensions are approximately 10 × 20 nm as expected and the height is ∼1.8 nm as is commonly observed for DNA duplexes in AFM. A significant proportion of the individual constructs on the mica surface (Figure 5a) displayed this naphthalene-like topology, and one of these is shown at higher resolution in Figure 5b. Given that the size of the hole in the middle of these structures should be around 4−5 nm and that they are indeed dynamic structures, it is not surprising that the hole is not evident in the images; tip convolution and the soft nature of DNA makes it rather difficult to obtain real nanometer lateral resolution in this case.

Discussion. The gel electrophoresis studies in Figure 2 conclusively prove the self-assembly of the nanostructures as designed. This fidelity to the self-assembly process with fast and efficient formation is imperative if the nanoconstructs are to serve any useful purpose. The steplike retardation of the bands in the gel upon addition of each new three-way node clearly indicates the binding of subsequent oligonucleotides and that all component strands are present in the final structure. Comparison to the faster-migrating band in lane **H** where one of the central nodes (**9**) is removed also indicates that the central "strut" between nodes **9** and **10** in the structure is double-stranded and that all peripheral edges of the construct are closed and double-stranded with the exception of the addition of the final three-way oligonucleotide (**8**) whose closure is evidenced by the binding of the TFO. The selective duplex addressability of each of the peripheral ten-mer arms is confirmed by the electrophoresis experiment in Figure 2b where eight individual addresses on the nanostructure can be individually targeted. This implies that eight specific addresses are distinguishable and most importantly available in an area just 10 × 20 nm giving rise to an extremely dense information content packing. In all cases, the yield is high, and differences in fluorescence intensity may be due to a change in environment and thus quantum yield of the fluorophore between the first four addresses and the final four addresses. The traces of other products are partly due to stoichiometric errors and partly due to a thermodynamically and kinetically governed distribution of species. Optimization of annealing procedure has previously shown the importance of kinetics in determining the yield of nanoconstruct.[14] The yield here is estimated from the fluorescence intensity in the gel volume as being 65−80%, which regarding the number of building blocks (18) corresponds to a hybridization efficiency of 98−99% in each step. It is from these eight peripheral arms that the nanostructure will be extended to form a nonrepetitive network, and therefore it is important to note that this also proves that extension of the addressable system is possible.

By lowering the pH of the buffered solution to 6.3, a triplex-forming strand composed of easily protonated bases can now add across a specific double-stranded sequence and form a stable tract of triplex DNA in the structure. This is illustrated in these studies by addressing the edge formed between nodes **6** and **7**, although full-recognition TFOs make it possible to selectively target any ten-mer duplex sequence in the construct.[16] This interaction can clearly be seen in Figure 3 where the triplex-forming strand, labeled by Cy3, migrates with the naphthalene construct (**T6**) labeled with Cy5. The nonbound triplex-forming strand appears as a much slower moving diffuse band. There can be no doubt that there is triplex formation at this pH and that the interaction can be terminated by increasing the pH to 7.5 where the triplex strand is now destabilized and comes apart from the structure. This is confirmed by the FRET results presented in Figure 4 where the TFO is seen to bind to its target on the nanostructure. Furthermore, it is possible to associate and dissociate the TFO repeatedly by switching the pH between 6 and 8. Thus, we have qualitatively shown that we can bind a TFO to its target site in our nanoconstruct. At this point, our goal is to show that TFO technology can be used to selectively address nonrepetitive small unit cell size DNA nanonetworks and that pH can be used as a way of controlling this rather than to have a quantitative binding. However, it is worth mentioning that we only use a 25% excess of TFO strand, while it is common to use a much larger excess for TFO-binding (up to 1000%) to ensure quantitative labeling.[16] Consequently, we do not expect to have quantitative labeling although allowing for the reduction in the intensity of the band due to FRET and comparison of the intensities of the bands in **G** and **T6** would suggest that

a large proportion is bound. In Figure 4, one can see that the intensity of the FRET signal decreases after each cycle (compare pH6A, pH6B, and pH6C). A similar decrease in Cy5 intensity can be observed when selectively exciting only Cy5 in the same samples (see Supporting Information). This indicates that we lose some material in each change in pH. The loss is most likely a result of the aggressive way in which the pH is being changed.

If one sees the addition of protons to the system (lowering the pH) as the input signal, then the information is both written and automatically locked by the stability of the triplex. Energy transfer is then the output signal that indicates this process has occurred and that represents the information encoded by the triplex strand that can be read at any time by fluorescence measurements. The "memory" can be erased by simply raising the pH again. This is easily demonstrated by cycling the system between the two states, pH 6 and 8, as shown in Figure 4. This does not merely prove the write−lock−read−erase mechanism but also shows the general reversibility of these addressable systems and that the cycle can efficiently be repeated. In a larger array, many full-recognition triplex-forming strands, individually labeled with distinct chromophores, could be used to store information spatially and even immobilized on a surface. The fact that the fluorophores or other moieties can be so precisely located in 2D space also means that one can easily build an array with carefully spaced functionalities in specific patterns/directions to build electron and energy transfer circuits. This is an important application of our nanostructure strategies and represents a fundamental shift away from the lithographic approaches currently used. Alternatively, one can envisage a system where an addressable network is selectively patterned by nanoparticles using pH-controlled triplex recognition, and this specific pattern is transferred to a surface before the network template is removed by a change in pH again. Nanoarrays based on these unit cells would possess a very fine mesh size, and such a kind of reusable mask would prove an extremely useful complement to lithographic approaches that are currently limited in their spatial precision.

Conclusions. Here, we prove the intrinsic usefulness of the newly developed three-way oligonucleotide building blocks to form nonrepetitive, selectively addressable nanostructures that can easily be functionalized with subnanometer precision. The write−lock−read−erase function of the system is confirmed by the fluorescence measurements that can be repeated in several cycles without loss of detection sensitivity. Larger networks will certainly provide a basis for novel nanocircuits constructed with near Ångström-scale precision. With the incorporation of other suitable functionalities, such as catalytic moieties, it may even be possible to carry out chemical reactions in specific directions, as a nanoscale assembly line. A further likely use is as a nanotemplate where a network could be used as a stencil for deposition of nanoparticles onto a surface in a specific pattern, dictated by the addressability and triplex recognition and removal of the template DNA by pH switching for reuse. To fully exploit the addressability of these structures, it would be most interesting to immobilize them on various surfaces, for example, gold or nanofabricated surfaces[25] but even by tethering to lipid bilayers via hydrophobic linkers.[26,27] Exploration of their reinforcement via chemical cross-linking may also prove useful.[28] Work is currently underway to deliver such systems where simple energy transfer circuits incorporated into networks based on these trigonal nodes can be self-assembled in solution before surface deposition.

Acknowledgment. Professor Björn Åkerman is gratefully acknowledged for discussions and advice regarding gel electrophoresis. This research is funded by the European Commission's Sixth Framework Programme (Project Reference AMNA, Contract No. 013575)

Supporting Information Available: Oligonucleotide sequences, FRET spectra and data analysis, AFM sample preparation. This material is available free of charge via the Internet at http://pubs.acs.org.

References

(1) Mathieu, F.; Liao, S. P.; Kopatscht, J.; Wang, T.; Mao, C. D.; Seeman, N. C. *Nano Lett.* **2005**, *5*, 661−665.
(2) Seeman, N. C. *Nature* **2003**, *421*, 427−31.
(3) Winfree, E.; Liu, F. R.; Wenzler, L. A.; Seeman, N. C. *Nature* **1998**, *394*, 539−544.
(4) Goodman, R. P.; Schaap, I. A. T.; Tardin, C. F.; Erben, C. M.; Berry, R. M.; Schmidt, C. F.; Turberfield, A. J. *Science* **2005**, *310*, 1661−1665.
(5) Shih, W. M.; Quispe, J. D.; Joyce, G. F. *Nature* **2004**, *427*, 618−621.
(6) Erben, C. M.; Goodman, R. P.; Turberfield, A. J. *J. Am. Chem. Soc.* **2007**, *129*, 6992−6993.
(7) Mitchell, J. C.; Harris, J. R.; Malo, J.; Bath, J.; Turberfield, A. J. *J. Am. Chem. Soc.* **2004**, *126*, 16342−16343.
(8) Rothemund, P. W. K.; Ekani-Nkodo, A.; Papadakis, N.; Kumar, A.; Fygenson, D. K.; Winfree, E. *J. Am. Chem. Soc.* **2004**, *126*, 16344−16352.
(9) Chworos, A.; Severcan, I.; Koyfman, A. Y.; Weinkam, P.; Oroudjev, E.; Hansma, H. G.; Jaeger, L. *Science* **2004**, *306*, 2068−2072.
(10) Macdonald, J.; Li, Y.; Sutovic, M.; Lederman, H.; Pendri, K.; Lu, W. H.; Andrews, B. L.; Stefanovic, D.; Stojanovic, M. N. *Nano Lett.* **2006**, *6*, 2598−2603.
(11) Aldaye, F. A.; Sleiman, H. F. *Angew. Chem., Int. Ed.* **2006**, *45*, 2204−2209.
(12) Aldaye, F. A.; Sleiman, H. F. *J. Am. Chem. Soc.* **2007**, *129*, 4130−4131.
(13) Lund, K.; Liu, Y.; Lindsay, S.; Yan, H. *J. Am. Chem. Soc.* **2005**, *127*, 17606−17607.
(14) Tumpane, J.; Sandin, P.; Kumar, R.; Powers, V. E. C.; Lundberg, E. P.; Gale, N.; Baglioni, P.; Lehn, J.-M.; Albinsson, B.; Lincoln, P.; Wilhelmsson, L. M.; Brown, T.; Norden, B. *Chem. Phys. Lett.* **2007**, *440*, 125−129.
(15) Scheffler, M.; Dorenbeck, A.; Jordan, S.; Wustefeld, M.; von Kiedrowski, G. *Angew. Chem., Int. Ed.* **1999**, *38*, 3312−3315.
(16) Rusling, D. A.; Powers, V. E. C.; Ranasinghe, R. T.; Wang, Y.; Osborne, S. D.; Brown, T.; Fox, K. R. *Nucleic Acids Res.* **2005**, *33*, 3025−3032.
(17) Cuenoud, B.; Casset, F.; Husken, D.; Natt, F.; Wolf, R. M.; Altmann, K. H.; Martin, P.; Moser, H. E. *Angew. Chem., Int. Ed* **1998**, *37*, 1288−1291.
(18) Cassidy, S. A.; Slickers, P.; Trent, J. O.; Capaldi, D. C.; Roselt, P. D.; Reese, C. B.; Neidle, S.; Fox, K. R. *Nucleic Acids Res.* **1997**, *25*, 4891−4898.
(19) Hildbrand, S.; Blaser, A.; Parel, S. P.; Leumann, C. J. *J. Am. Chem. Soc.* **1997**, *119*, 5499−5511.
(20) Buchini, S.; Leumann, C. J. *Angew. Chem., Int. Ed.* **2004**, *43*, 3925−3928.
(21) Blommers, M. J. J.; Natt, F.; Jahnke, W.; Cuenoud, B. *Biochemistry* **1998**, *37*, 17714−17725.
(22) Chen, Y.; Lee, S. H.; Mao, C. *Angew. Chem., Int. Ed.* **2004**, *43*, 5335−5338.

(23) Jung, Y. H.; Lee, K. B.; Kim, Y. G.; Choi, I. S. *Angew. Chem., Int. Ed.* **2006**, *45*, 5960−5963.
(24) Rusling, D. A.; Le Strat, L.; Powers, V. E. C.; Broughton-Head, V. J.; Booth, J.; Lack, O.; Brown, T.; Fox, K. R. *FEBS Lett.* **2005**, *579*, 6616−6620.
(25) Erkan, Y.; Czolkos, I.; Jesorka, A.; Wilhelmsson, L. M.; Orwar, O. *Langmuir* **2007**, *23*, 5259−5263.
(26) Benkoski, J. J.; Hook, F. *J. Phys. Chem. B* **2005**, *109*, 9773−9779.
(27) Banchelli, M.; Berti, D.; Baglioni, P. *Angew. Chem., Int. Ed.* **2007**, *46*, 3070−3073.
(28) Kumar, R.; El-Sagheer, A.; Tumpane, J.; Lincoln, P.; Wilhelmsson, L. M.; Brown, T. *J. Am. Chem. Soc.* **2007**, *129*, 6859−6864.

NL072512I